Probing the Influence of Local Coordination Environment on the Properties of Fe-Type Nitrile Hydratase Model Complexes

Henry L. Jackson, Steven C. Shoner, Durrell Rittenberg, Jerry A. Cowen,† Scott Lovell,‡ David Barnhart,‡ and Julie A. Kovacs*

Department of Chemistry, University of Washington, Seattle, Washington 98195

Received September 27, 2000

A series of four structurally related *cis*-dithiolate-ligated Fe(III) complexes, $[Fe^{III}(DITpy)_2]Cl$ (**1**), $[Fe^{III}(DITIm)_2]Cl$ (**2**), $[Fe^{III}(ADIT)_2]Cl$ (**3**), and $[Fe^{III}(AMIT)_2]Cl$ (**4**), are described. The structural characterization of **3** as well as the spectroscopic properties of **3** and **4** has been previously reported. Crystal data for **1**, **2**, and **4** are as follows: **1**·$3H_2O$ crystallizes in the orthorhombic space group $Pca2_1$ with $a = 19.800(4)$ Å, $b = 18.450(4)$ Å, $c = 14.800(3)$ Å, and $Z = 8$. **2**·$^1/_2EtOH$·$^1/_2H_2O$ crystallizes in the monoclinic space group C_c with $a = 24.792(4)$ Å, $b = 14.364(3)$ Å, $c = 17.527(3)$ Å, $\beta = 124.91(2)°$, and $Z = 8$. **4** crystallizes in the triclinic space group $P\bar{1}$ with $a = 8.0152(6)$ Å, $b = 10.0221(8)$ Å, $c = 11.8384(10)$ Å, $\alpha = 73.460(3)°$, $\beta = 71.451(5)°$, $\gamma = 72.856(4)°$, and $Z = 2$. Complexes **1**−**4** share a common S_2N_4 coordination environment that consists of two *cis*-thiolates, two *trans*-imines, and two *cis*-terminal nitrogen donors: N_{term} = pyridine (**1**), imidazole (**2**), and primary amine (**3** and **4**). The crystallographically determined mean Fe−S bond distances in **1**−**4** range from 2.196 to 2.232 Å and are characteristic of low-spin Fe(III)−thiolate complexes. The low-spin $S = {}^1/_2$ ground state was confirmed by both EPR and magnetic susceptibility measurements. The electronic spectra of these complexes are characterized by broad absorption bands centered near ∼700 nm that are consistent with ligand-to-metal charge-transfer (CT) bands. The complexes were further characterized by cyclic voltammetry measurements, and all possess highly negative Fe(III)/Fe(II) redox couples (∼ −1 V vs SCE, saturated calomel electrode) indicating that alkyl thiolate donors are effective at stabilizing Fe(III) centers. Both the redox couple and the 700 nm band in the visible spectra show solvent-dependent shifts that are dependent upon the H-bonding ability of the solvent. The implications of these results with respect to the active site of the iron-containing nitrile hydratases are also discussed.

Introduction

The coordination chemistry of alkyl thiolate ligated iron(III) compounds are of interest as several mononuclear non-heme iron metalloenzymes, including nitrile hydratase,[1] neelaredoxin,[2] and desulfoferrodoxin,[3] have been shown to contain cysteine-ligated iron. This is in contrast to the majority of non-heme iron enzymes that contain exclusively nitrogen and/or oxygen donors.[4] Higher oxidation state transition metal thiolates are uncommon, as they are unstable to intramolecular electron transfer affording disulfides and reduced metal species.[5] For this reason, only a small number of Fe(III) thiolate complexes have been reported, and even fewer have been structurally characterized.[6] Many of these complexes contain less reducing aromatic thiolates.

Nitrile hydratases (NHases) are mononuclear iron-containing bacterial metalloenzymes that catalyze the hydration of nitriles to amides.[1] Less is known about the function of neelaredoxin[7] and desulfoferrodoxin.[8] Certain species of bacteria produce

* Author to whom correspondence should be addressed: Dr. Julie A. Kovacs, Department of Chemistry, University of Washington, Box 351700, Seattle, WA 98195-1700. E-mail: kovacs@chem.washington.edu. Fax: 206-685-8665.

† Deceased, Department of Physics, Michigan State University, East Lansing, MI 48824.

‡ UW staff crystallographers.

(1) Kobayashi, M.; Shimizu, S. *Nature Biotechnology* **1998**, *16*, 733−736.

(2) Chen, L.; Sharma, P.; LeGall, J.; Mariano, A. M.; Teixeira, M.; Xavier, A. V. *Eur. J. Biochem.* **1994**, *226*, 613−618.

(3) Tavares, P.; Ravi, N.; Moura, J. J. G.; LeGall, J.; Huang, Y.-H.; Crouse, B. R.; Johnson, M. K.; Huynh, B. H.; Moura, I. *J. Biol. Chem.* **1994**, *269*, 10504−10510.

(4) (a) Que, L., Jr.; Ho, R. Y. N. *Chem. Rev.* **1996**, *96*, 2607−2624. (b) Wallar, B. J.; Lipscomb, J. D. *Chem. Rev.* **1996**, *96*, 2625−2657. (c) Solomon, E. I.; Brunold, T. C.; Davis, M. I.; Kemsley, J. N.; Lee, S.; Lehnert, N.; Neese, F.; Skulan, A. J.; Yang, Y.; Zhou, J. *Chem. Rev.* **2000**, *100*, 235−350. (d) Feig, A. L.; Lippard, S. J. *Chem. Rev.* **1994**, *94*, 759−805.

(5) (a) Maelia, L. E.; Millar, M.; Koch, S. A. *Inorg. Chem.* **1992**, *31*, 4594−4600. (b) Millar, M.; Lee, J. F.; Fikar, R. *Inorg. Chim. Acta* **1996**, *243*, 333−343. (c) Herskovitz, T.; Depamphilis, B. V.; Gillum, W. O.; Holm, R. H. *Inorg. Chem.* **1975**, *14*, 1426−1430.

(6) (a) Noveron, J. C.; Herradora, R.; Olmstead, M. M.; Mascharak, P. K. *Inorg. Chim. Acta* **1999**, *285*, 269−276. (b) Shoner, S. C.; Barnhart, D.; Kovacs, J. A. *Inorg. Chem.* **1995**, *34*, 4517−4518. (c) Kopf, M.; Varech, D.; Tuchagues, J.; Mansuy, D.; Artaud, I. *J. Chem. Soc., Dalton Trans.* **1998**, 991−998. (d) Schweitzer, D.; Ellison, J. J.; Shoner, S. C.; Lovell, S.; Kovacs, J. A. *J. Am. Chem. Soc.* **1998**, *120*, 10996−10997. (e) Heinrich, L.; Li, Y.; Vaissermann, J.; Chottard, G.; Chottard, J. *Angew. Chem., Int. Ed.* **1999**, *38*, 3526−3528. (f) Ellison, J. J.; Nienstedt, A.; Shoner, S. C.; Barnhardt, D.; Cowen, J. A.; Kovacs, J. A. *J. Am. Chem. Soc.* **1998**, *120*, 5691−5700. (g) Artaud, I.; Chatel, S.; Chauvin, A. S.; Bonnet, D.; Kopf, M. A.; Leduc, P. *Coord. Chem. Rev.* **1999**, *192*, 577−586. (h) Noveron, J. C.; Olmstead, M. M.; Mascharak, P. K. *Inorg. Chem.* **1998**, *37*, 1138−1139. (i) Nivorozhkin, A. L.; Uraev, A. I.; Bondarenko, G. I.; Antsyshkina, A. S.; Kurbatov, V. P.; Garnovskii, A. D.; Turta, C. I.; Brashoveanu, N. D. *Chem. Commun. (Cambridge)* **1997**, *18*, 1711−1712. (j) Govindaswamy, N.; Quarless, D. A., Jr.; Koch, S. A. *J. Am. Chem. Soc.* **1995**, *117*, 8468−8469. (k) Beissel, T.; Buerger, K. S.; Voigt, G.; Wieghardt, K.; Butzlaff, C.; Trautwein, A. X. *Inorg. Chem.* **1993**, *32*, 124−126. (l) Fallon, G. D.; Gatehouse, B. M. *J. Chem. Soc., Dalton Trans.* **1975**, 1344−1347. (m) Fallon, G. D.; Gatehouse, B. M.; Marini, P. J.; Murray, K. S.; West, B. O. *J. Chem. Soc., Dalton Trans.* **1984**, 2733−2739. (n) Koch, W. O.; Schünemann, V.; Gerdan, M.; Trautwein, A. X.; Krüger, H. *Chem.—Eur. J.* **1998**, *4*, 686−691.

10.1021/ic001271d CCC: $20.00
Published on Web 02/27/2001

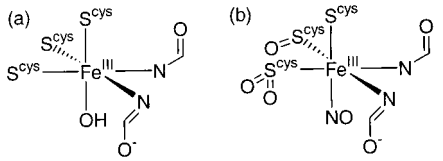

Figure 1. NHase active site as determined by X-ray crystallography: (a) photoactivated form determined at 2.65 Å resolution and (b) NO-inactivated form determined at 1.7 Å resolution.

NHases that contain cobalt[9] in place of iron. The iron-containing NHases (Fe-NHase) are inactivated upon exposure to nitric oxide (NO) in the dark and can be photoactivated upon exposure to light.[10] The Fe-NHases have been studied by a number of spectroscopic techniques. On the basis of EPR,[11] resonance Raman,[12] EXAFS,[13] and ENDOR[14] measurements, the active site was proposed to contain a six-coordinate, low-spin ($S = {}^1/_2$) ferric ion in a mixed N,O/S coordination environment. Recently, two separate groups independently determined the crystal structure of the Fe enzyme. The initial study was performed on the photoactivated form of the enzyme at a resolution of 2.65 Å.[15] The structure revealed a novel coordination environment that consists of two amide nitrogens provided by the peptide backbone and three cysteine-thiolate donors (Figure 1a). A more recent structure, at a resolution of 1.7 Å, of the NO-inhibited form revealed that two of the metal-bound sulfurs are post-translationally modified to sulfenate (Cys-SO^-) and sulfinate (Cys-SO_2^-) groups (Figure 1b).[16] Mass spectrometric studies[17] of tryptic digests of the active enzyme provide evidence in support of the proposed modification to Cys-SO_2^-, while evidence to support modification to Cys-SO^- was inconclusive. Oxidized sulfurs were not detected in the initial X-ray structure[15] or by resonance Raman.[12]

The Fe-NHases display unique electronic properties including a low-spin ($S = {}^1/_2$) ground state and a broad electronic absorption near 700 nm that has been shown to be a sulfur-to-iron charge-transfer band.[12,18,30] Both the EPR (Table 5) and the electronic spectral properties (Table 3) show pH- and substrate-dependent shifts. Treatment of Fe-NHases with common biological reductants such as dithiothreitol do not result in iron reduction, suggesting that the Fe(III) oxidation state is stable in this enzyme.[11]

Despite the structural advances, many questions about NHase remain unanswered. Given the apparent discrepancies between the two NHase X-ray structures, and spectroscopic data, alternative methods capable of providing additional information about the structure of this site are needed. Ultimately one would hope to correlate active-site structure with spectroscopic properties. One such approach is the synthetic modeling approach. Herein we report the synthesis, structure, and properties of a series of structurally related alkyl thiolate ligated Fe(III) complexes that closely model the spectroscopic properties of the non-heme iron site of nitrile hydratase, in spite of the absence of oxidized sulfurs.

Experimental Section

General Methods. All reactions were carried out under nitrogen at room temperature using standard Schlenk techniques or in a Vacuum Atmospheres inert atmosphere Dry Lab. Solvents were dried according to published procedures.[19] Hydrogen sulfide (Praxair) was used as received. All other reagents were purchased commercially (Aldrich) and used as received. 3-Methyl-3-mercapto-2-butanone was synthesized as described previously.[20]

Physical Methods. IR spectra were obtained on a Perkin-Elmer model 1640 FT-IR spectrophotometer, with samples prepared as KBr pellets. Electronic absorption spectra were recorded on a Hewlett-Packard model 8452A diode array spectrophotometer. NMR spectra were recorded on a Bruker AC-200 spectrometer and referenced to residual protio solvent. Solution magnetic moments were determined using Evan's method,[21] as corrected for superconducting solenoids.[22] Solid state magnetic susceptibility data were collected on a Quantum Design model MPMS SQUID magnetometer. Elemental analyses were performed by Galbraith Laboratories, Knoxville, TN, or Canadian Microanalytical Services, British Columbia, Canada. EPR spectra were recorded on an EPX Bruker spectrometer operating at X-band frequency. Cyclic voltammograms were obtained using an EG&G Princeton Applied Research (PAR) 273 potentiostat with a glassy carbon working electrode, a platinum wire counter electrode, and a SCE (saturated calomel electrode) reference electrode, and 0.1 M (n-Bu_4N)-(PF_6) (in MeCN) or 0.1 M KCl (in H_2O) as the supporting electrolyte.

Synthesis of $[Fe^{III}(DITpy)_2]Cl\cdot EtOH$ (1). 3-Methyl-3-mercapto-2-butanone (0.71 g, 6.0 mmol), 2-(aminomethyl)pyridine (0.65 g, 6.0 mmol) and NaOMe (0.32 g, 6.0 mmol) were dissolved in 30 mL of MeOH, and the resulting solution was stirred for 1.5 h. In a separate flask, anhydrous $FeCl_3$ (0.49 g, 3.0 mmol) was dissolved in 30 mL of MeOH and filtered through a bed of Celite. The solutions were cooled to −35 °C, and the $FeCl_3$ solution was added to the thiolate/amine solution dropwise. The resulting reaction mixture was stirred for 1.5 h at room temperature. Solvent was removed under reduced pressure to afford an orange-brown solid that was extracted with 20 mL of MeCN and filtered through a bed of Celite to remove NaCl and other insoluble impurities. Removal of solvent under reduced pressure followed by a

(7) Silva, G.; Oliveira, S.; Gomes, C. M.; Pacheco, I.; Liu, M. Y.; Xavier, A. V.; Teixeira, M.; Le Gall, J.; Rodriques-Pousada, C. *Eur. J. Biochem.* **1999**, *259*, 235−243.
(8) Romão, C. V.; Liu, M. Y.; Le Gall, J.; Gomes, C. M.; Braga, V.; Pacheco, I.; Xavier, A. V.; Teixeira, M. *Eur. J. Biochem.* **1999**, *261*, 438−443.
(9) (a) Brennan, B. A.; Alms, G.; Scarrow, R. C. *J. Am. Chem. Soc.* **1996**, *118*, 9194−9195. (b) Pogorelova, T. E.; Ryabchenko, L. E.; Yanenko, A. S. *FEMS Microbiol. Lett.* **1996**, *144*, 191−195. (c) Nagasawa, T.; Takeuchi, K.; Yamada, H. *Eur. J. Biochem.* **1991**, *196*, 581−589.
(10) (a) Odaka, M.; Fujii, K.; Hoshino, M.; Noguchi, T.; Tsujimura, M.; Nagashima, S.; Yohda, N.; Nagamune, T.; Inoue, I.; Endo, I. *J. Am. Chem. Soc.* **1997**, *119*, 3785−3791. (b) Noguchi, T.; Hoshino, M.; Tsujimura, M.; Odaka, M.; Inoue, Y.; Endo, I. *Biochemistry* **1996**, *35*, 16777−16781. (c) Bonnet, D.; Artaud, I.; Moali, C.; Pétré, D.; Mansuy, D. *FEBS Lett.* **1997**, *409*, 216−220. (d) Noguchi, T.; Honda, J.; Nagamune, T.; Sasabe, H.; Inoue, Y.; Endo, I. *FEBS Lett.* **1995**, *358*, 9−12.
(11) Sugiura, Y.; Kuwahara, J.; Nagasawa, T.; Yamada, H. *J. Am. Chem. Soc.* **1987**, *109*, 5848−5850.
(12) Brennan, B. A.; Cummings, J. G.; Chase, D. B.; Turner, I. M., Jr.; Nelson, M. J. *Biochemistry* **1996**, *35*, 10068−10077.
(13) Scarrow, R. C.; Brennan, B. A.; Cummings, J. G.; Jin, H.; Duong, D. J.; Kindt, J. T.; Nelson, M. J. *Biochemistry* **1996**, *35*, 10078−10088.
(14) (a) Jin, H.; Turner, I. M., Jr.; Nelson, M. J.; Gurbriel, R. J.; Doan, P. E.; Hoffman, B. M. *J. Am. Chem. Soc.* **1993**, *115*, 5290−5291. (b) Doan, P. E.; Nelson, M. J.; Jin, H.; Hoffman, B. M. *J. Am. Chem. Soc.* **1996**, *118*, 7014−7015.
(15) Huang, W.; Cummings, J.; Nelson, M.; Schneider, G.; Lindqvist, Y. *Structure* **1997**, *5*, 691−699.
(16) Nagashima, S.; Nakasako, M.; Dohmae, N.; Tsujimura, M.; Takio, K.; Odaka, M.; Yohda, M.; Kamiya, N.; Endo, I. *Nature Struct. Biol.* **1998**, *5*, 347−351.
(17) (a) Tsujimura, M.; Dohmae, N.; Odaka, M.; Chijimatsu, M.; Takio, K.; Yohda, M.; Hoshino, M.; Nagashima, S.; Endo, I. *J. Biol. Chem.* **1997**, *272*, 29454−29459. (b) Nojiri, M.; Yohda, M.; Odaka, M.; Matsushita, Y.; Tsujimura, M.; Yoshida, T.; Dohmae, N.; Takio, K.; Endo, I. *J. Biochem.* **1999**, *125*, 696−704. (c) Murakami, T.; Nojiri, M.; Nakayama, H.; Odaka, M.; Yohda, M.; Dohmae, N.; Takio, K.; Nagamune, T.; Endo, I. *Protein Sci.* **2000**, *9*, 1024−1030.
(18) Nagasawa, T.; Ryuno, K.; Yamada, H. *Biochem. Biophys. Res. Commun.* **1986**, *139*, 1305−1312.
(19) Perrin, D. D.; Armarego, W. L. F. *Purification of Laboratory Chemicals*; Pergamon Press: New York, 1988.
(20) Shoner, S. C.; Nienstedt, A. M.; Ellison, J. J.; Kung, I. Y.; Barnhart, D.; Kovacs, J. A. *Inorg. Chem.* **1998**, *37*, 5721−5726.
(21) Evans, D. A. *J. Chem. Soc.* **1959**, 2003−2005.
(22) Live, D. H.; Chan, S. I. *Anal. Chem.* **1970**, *42*, 791−792.

second extraction with 24 mL of an Et_2O/EtOH mixture (1:1 (v/v)) and filtration through a bed of Celite gave an orange-brown filtrate, to which was added 20 mL of Et_2O. The resulting solution was stored in a freezer (−35 °C) overnight to afford **1** as dark block-shaped crystals. Yield: 0.84 g (51%). μ_{eff} = 2.3 μ_B in MeOH solution at ambient temperature (298 K). FT-IR (KBr pellet) ν(cm^{-1}): 1626 (imine). Anal. Calcd for $FeC_{24}H_{36}N_4OS_2Cl$: C, 52.22; H, 6.57; N, 10.15. Found: C, 51.97; H, 6.72; N, 10.15. Absorption spectrum: (MeOH) λ_{max} (nm) (ϵ_M) = 360 (3100), 456 (2200), 780 (1300); (MeCN): λ_{max} (nm) (ϵ_M) = 362 (3200), 458 (2300), 784 (1300); (H_2O) λ_{max} (nm) (ϵ_M) = 458 (2000), 732 (1400).

Synthesis of [Fe^{III}(DITIm)$_2$]Cl·$^1/_2$EtOH·$^1/_2$H$_2$O (2). 3-Methyl-3-mercapto-2-butanone (0.71 g, 6.0 mmol), histamine dihydrochloride (1.1 g, 6.0 mmol), and NaOH (0.72 g, 18 mmol) were dissolved in 80 mL of MeOH, and the resulting solution was stirred for 45 min. In a separate flask, anhydrous $FeCl_3$ (0.49 g, 3.0 mmol) was dissolved in 40 mL of MeOH and filtered through a bed of Celite. The solutions were cooled to −35 °C, and the $FeCl_3$ solution was added to the thiolate/amine. The resulting reaction mixture was stirred for 1.5 h at room temperature. Removal of solvent under reduced pressure afforded a maroon solid that was extracted with 60 mL of a MeOH/MeCN mixture (1:5 (v/v)) and filtered through a bed of Celite to remove NaCl and other insoluble impurities. Removal of solvent under reduced pressure followed by a second extraction with 45 mL of an Et_2O/EtOH mixture (1:2 (v/v)) and filtration through a bed of Celite gave an orange-brown filtrate, which was layered with 15 mL of Et_2O. The resulting solution was stored in a freezer (−35 °C) for 3 days to afford a dark maroon microcrystalline solid. Recrystallization from EtOH/Et_2O in a freezer (−35 °C) overnight afforded **2** as a dark maroon microcrystalline solid. Yield: 0.26 g (16%). μ_{eff} = 2.4 μ_B in MeOH solution at ambient temperature (298 K). FT-IR (KBr pellet) ν(cm^{-1}): 1600 (imine). Anal. Calcd for $FeC_{21}H_{36}N_6OS_2Cl$: C, 46.37; H, 6.67; N, 15.45. Found: C, 46.48; H, 6.65; N, 15.10. Absorption spectrum: (MeOH) λ_{max}(nm) (ϵ_M) = 466 (1300), 796 (1200); (MeCN) λ_{max} (nm) (ϵ_M) = 466 (1400), 802 (1200); (H_2O) λ_{max} (nm) (ϵ_M) = 458 (1200), 740 (1200).

[Fe^{III}(ADIT)$_2$]Cl (**3**) and [Fe^{III}(AMIT)$_2$]Cl (**4**) were synthesized as described previously.[23]

X-ray Crystallographic Structure Determinations. Crystals of **1**, **2**, and **4** were immersed in Paratone oil inside a glovebox, and then a suitable crystal of each was mounted on a glass fiber with silicon grease and immediately placed in a low-temperature N_2(g) stream. X-ray data for **1** and **2** was collected at −90 °C using an Enraf-Nonius CAD4 diffractometer (Mo Kα, λ = 0.71073 Å) equipped with a low-temperature device. X-ray data for **4** was collected at −112 °C using a Nonius Kappa CCD diffractometer (Mo Kα, λ = 0.71070 Å) equipped with a low-temperature device. X-ray data collection parameters are summarized in Table 1.

Cell constants for **1** and an orientation matrix were obtained by the standard method from 25 reflections at −90 °C on a CAD4 diffractometer. Systematic absences and subsequent least-squares refinement were used to uniquely define the space group as $Pca2_1$. During data collection the intensities of several representative reflections were measured as a check on crystal stability, and there was no loss of intensity during data collection. Equivalent reflections were merged, and only those for which $I_o > 2\sigma(I)$ were included in the refinement. The weighting scheme used was $[\alpha^2F_o^2]^{-1}$. The structure was solved primarily from difference maps, with initial refinement on the iron atom obtained from a Patterson map. Hydrogens were introduced by calculation and refined using a riding model. Final full-matrix refinement gave an R value of 5.84% for 564 parameters with 3442 observed reflections with $F > 4.0\sigma(F)$.

Cell constants for **2** and an orientation matrix were obtained by the standard method from 25 reflections at −90 °C on a CAD4 diffractometer. Systematic absences and subsequent least-squares refinement were used to uniquely define the space group as C_c. During data collection the intensities of several representative reflections were measured as a check on crystal stability, and there was no loss of intensity during data collection. Equivalent reflections were merged, and only those for which $I_o > 2\sigma(I)$ were included in the refinement. The weighting scheme used was $[\alpha^2F_o^2]^{-1}$. The structure was solved primarily from difference maps, with initial refinement on the iron atom obtained from a Patterson map. Hydrogen atoms were introduced by calculation and refined using a riding model. Final full-matrix least-squares refinement gave an R value of 3.92% for 576 parameters with 2883 observed reflections with $F > 4.0\sigma(F)$.

Table 1. Crystal Data, Intensity Collections,[a] and Structure Refinement Parameters for [Fe^{III}(DITpy)$_2$]Cl·3H$_2$O (**1**), [Fe^{III}(DITIm)$_2$]Cl·$^1/_2$EtOH·$^1/_2$H$_2$O (**2**), and [Fe^{III}(AMIT)$_2$]Cl (**4**)

	1	**2**	**4**
formula	$FeC_{22}H_{36}N_4O_3S_2Cl$	$FeC_{21}H_{36}N_6OS_2Cl$	$FeC_{10}H_{20}N_4S_2Cl$
mol wt	555.49	543.98	351.72
temp, K	183	183	161(2)
unit cell	orthorhombic	monoclinic	triclinic
a, Å	19.800(4)	24.792(4)	8.0152(6)
b, Å	18.450(4)	14.364(3)	10.0221(8)
c, Å	14.800(3)	17.527(3)	11.8384(10)
α, deg	90	90	73.460(3)
β, deg	90	124.91(2)	71.451(5)
γ, deg	90	90	72.856(4)
V, Å^3	5406(1)	5118(1)	842.16(12)
Z	8	8	2
D(calc), g/cm^3	1.361	2.824	1.387
space group	$Pca2_1$	C_c	$P\bar{1}$
R	0.0581[b]	0.0392[b]	0.0844[b]
R_w	0.0765[c]	0.0407[c]	0.2715[d]
GOF	1.62	1.08	1.064

[a] Mo Kα (λ = 0.71073 Å for **1** and **2**, 0.71070 Å for **4**) radiation; graphite monochromator; −90 °C. [b] $R = \sum||F_o| - |F_c||/\sum|F_o|$. [c] $R_w = [\sum w(|F_o| - |F_c|)^2/\sum wF_o^2]^{1/2}$, where $w^{-1} = [\sigma^2_{count} + (0.05F^2)^2]/4F^2$. [d] $R_w = \{\sum[w(F_o^2 - F_c^2)^2]/\sum[w(F_o^2)^2]\}^{1/2}$; $w = 1/[\sigma^2(F_o^2) + (0.1395P)^2 + 1.3703P]$, where $P = [F_o^2 + 2F_c^2]/3$.

Cell constants and the orientation matrix for data collection for **4** were obtained from 15 images exposed for 60 s at −112 °C on a Nonius Kappa CCD diffractometer. The systematic absences determined the space group $P\bar{1}$. The structure was solved by direct methods and expanded using Fourier techniques using the SIR92[24] software package. Integration of intensities and cell refinement for Kappa CCD data was carried out with DENZO and HKL SCALEPACK,[25] respectively. An empirical absorption correction was applied with SORTAV.[26] The structure was solved by direct methods and refined with SHELXL-97.[27] All non-hydrogen atoms were refined anisotropically by full-matrix least-squares. All hydrogen atoms were placed with idealized geometry except for the H's on N1 and N2, which were located by difference Fourier synthesis. All hydrogen atoms were refined with a riding model and U_{iso} values fixed such that they were 1.1U_{eq} of their parent atom and 1.5U_{eq} for methyl hydrogens. The final R factor was (R = 8.44%). There was a residual electron density peak of 2.452 e/Å^3 that could not be explained.

Results and Discussion

Synthesis. Six-coordinate [Fe^{III}(DITpy)$_2$]$^+$ (**1**), [Fe^{III}(DITIm)$_2$]$^+$ (**2**), [Fe^{III}(ADIT)$_2$]$^+$ (**3**),[23] and [Fe^{III}(AMIT)$_2$]$^+$ (**4**)[23] were prepared using a "one-pot" synthesis involving a metal-templated Schiff base condensation as illustrated in Scheme 1. In contrast to previously reported five-coordinate Fe(III) thiolate complexes (e.g., [Fe^{III}($S_2^{Me2}N_3$(Pr,Pr))]$^+$),[6f] complexes **1**−**4** can be synthesized directly from iron(III) chloride, without prior isolation of the iron(II) intermediate. In a typical reaction, 1 equiv of iron(III) chloride is added to a stirred solution of 2

(23) Shoner, S. C.; Barnhart, D.; Kovacs, J. A. *Inorg. Chem.* **1995**, *34*, 4517−4518.

(24) Altomare, A.; Cascarano, G.; Giacovazzo, C.; Burla, M. C.; Polidori, G.; Camalli, M. *J. Appl. Crystallogr.* **1994**, *27*, 435−442.

(25) Otinowski, Z.; Minor, W. *Methods Enzymol.* **1996**, *276*, 307−326.

(26) Blessing, R. H. *Acta Crystallogr.* **1995**, *A51*, 33−38.

(27) Sheldrick, G. M. *SHELXL97, Program for the Refinement of Crystal Structures*; University of Göttingen: Göttingen, Germany.

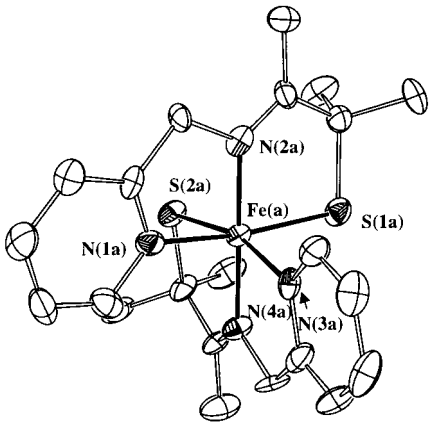

Figure 2. ORTEP plot of $[Fe^{III}(DITpy)_2]^+$ (**1**) showing 50% probability ellipsoids and atom-labeling scheme. H atoms have been omitted for clarity. For comparison purposes, atom labels were changed in Table 2 as follows: S(1a) = S(1), S(2a) = S(2), N(1a) = N^{t1}, N(3a) = N^{t2}, N(2a) = N^{im1}, N(4a) = N^{im2}.

Scheme 1

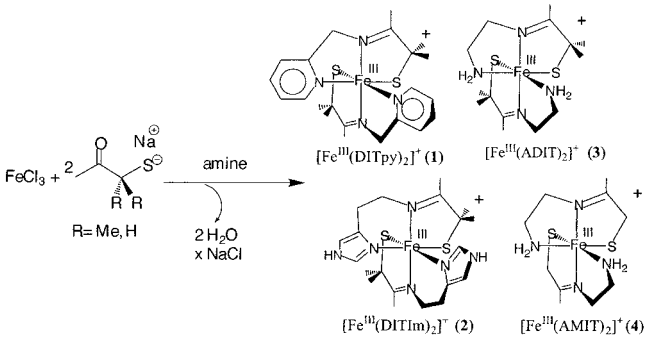

equiv each of a primary amine, the α-mercapto ketone, and sodium methoxide. In each case, reactions are carried out at −35 °C to minimize the formation of side products. Two methyl groups were included at the carbon α to the sulfurs in **1**−**3**, as bulky groups have been shown to stabilize higher oxidation state metal−thiolates.[28] This is illustrated by complex **4**, which lacks *gem*-dimethyl groups and decomposes more readily than complexes **1**−**3**.

X-ray Crystal Structures. Single crystals of **1**·$3H_2O$, **2**·$^1/_2$EtOH·$^1/_2H_2O$, and **4** were isolated from Et_2O-layered EtOH solutions. ORTEP diagrams of monocationic **1**, **2**, and **4** are shown in Figures 2, 3, and 4, respectively. The structure of monocationic **3** was described previously.[23] Metrical parameters for **1**−**4** are summarized in Table 2.[29] The iron in structures **1**−**4** is contained in a pseudo-octahedral bis(tris-chelated) environment, ligated by two *trans*-imines, two *cis*-thiolates, and either terminal pyridines (py) (**1**), imidazoles (Im) (**2**), or amines (NH_2) (**3** and **4**). The complexes exist as pairs of enantiomers, with both enantiomers present in the unit cell. Each of these complexes possesses extremely short Fe−S bond distances of approximately 2.20 Å, which are similar to the Fe−S bond distances reported for Fe-NHase.[15,16] These short distances are indicative of the low-spin state of Fe in these complexes. Prior to 1994, the range of 2.3−2.4 Å was considered to be the normal range for an Fe(III)−S bond.[5a,c] More recent work has shown that this range is only typical for high-spin Fe(III).[6] Replacing

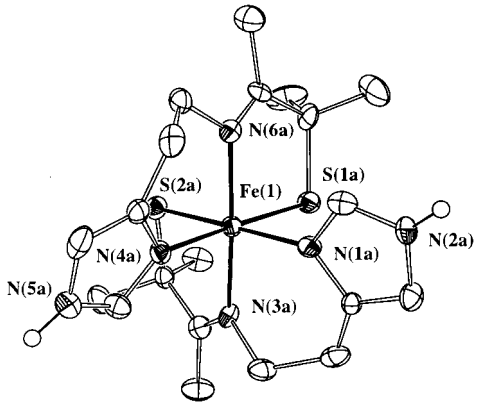

Figure 3. ORTEP plot of $[Fe^{III}(DITIm)_2]^+$ (**2**) showing 50% probability ellipsoids and atom-labeling scheme. H atoms, except for the imidazole N−H protons, have been omitted for clarity. For comparison purposes, atom labels were changed in Table 2 as follows: S(1A) = S(1), S(2a) = S(2), N(4a) = N^{t1}, N(1a) = N^{t2}, N(6a) = N^{im1}, N(3a) = N^{im2}.

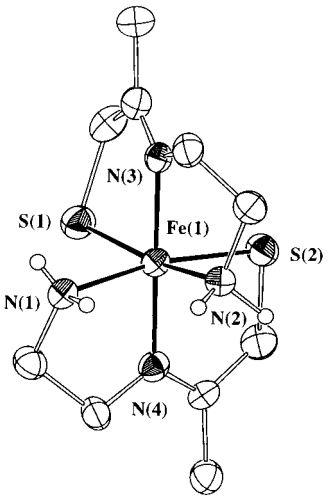

Figure 4. ORTEP plot of $[Fe^{III}(AMIT)_2]^+$ (**4**) showing 50% probability ellipsoids and atom-labeling scheme. H atoms, except for the amine N−H protons, have been omitted for clarity. For comparison purposes, atom labels were changed in Table 2 as follows: N(1) = N^{t1}, N(2) = N^{t2}, N(3) = N^{im1}, N(4) = N^{im2}.

the methyl substituents adjacent to the sulfurs in **1**−**3** with hydrogens in **4** results in longer (by ∼0.03 Å) Fe−S bonds: the mean Fe−S distance in **4** is the longest reported for a low-spin, six-coordinate Fe(III)−thiolate. The terminal nitrogen (N_{term}) donor type, on the other hand, has a negligible effect on the Fe−S distances. The mean Fe(III)−N_{im} (im = imine) bond distances in **1**, **2**, and **4** (1.922(6), 1.976(5), and 1.940(4) Å, respectively) are within the range of previously reported Fe(III)−N_{im} distances of similar six-coordinate, low-spin Fe(III) complexes.[6a,b,d,f,l] The chelate rings in structures **1** and **4** are all five-membered, with mean N_{im}−Fe−N_{term} bond angles of 82.2(1)° and 83.8(4)°, respectively, and N_{im}−Fe−S bond angles of 86.0(1)° and 86.6(1)°, respectively. The tris-chelates of structure **2**, on the other hand, are composed of one six-membered ring and one five-membered ring, with a N_{im}−Fe−N_{term} bond angle of 93.7(1)° and a N_{im}−Fe−S bond angle of 86.0(1)°. The larger chelate rings in **2** result in a less distorted structure; trans angles vary from 172.9(3)° to 179.3(2)° in **2** vs 164.1(2)° to 179.8(4)° in **1**.

Electronic Spectral Properties. Complexes **1**−**4** are all soluble in a wide variety of solvents, including water. Solutions are intensely colored due to absorption features with λ_{max} ∼700 nm, and extinction coefficients ($\epsilon \sim 1200\ M^{-1}\ cm^{-1}$) that are

(28) Millar, M.; Lee, J. F.; Koch, S. A.; Fikar, R. *Inorg. Chem.* **1982**, *21*, 4105−4106.

(29) Due to the platelike nature of the crystals of **4** its structure was of poorer quality than **1** and **2**.

Table 2. Selected Bond Distances (Å) and Bond Angles (deg) for $[Fe^{III}(DITpy)_2]^+$ (**1**), $[Fe^{III}(DITIm)_2]^+$ (**2**), $[Fe^{III}(ADIT)_2]^+$ (**3**), $[Fe^{III}(AMIT)_2]^+$ (**4**)[a]

	1	2	3	4
		Distances		
Fe−S(1)	2.202(3)	2.209(2)	2.200(1)	2.234(2)
Fe−S(2)	2.189(3)	2.213(2)	2.207(1)	2.231(2)
Fe−N^{t1}	2.014(8)[b]	2.039(7)	2.043(3)	2.054(6)
Fe−N^{t2}	2.032(8)	2.076(7)	2.059(3)	2.052(6)
Fe−N^{im1}	1.934(8)[c]	1.974(7)	1.938(2)	1.950(6)
Fe−N^{im2}	1.909(8)	1.978(7)	1.938(2)	1.930(6)
		Angles		
N^{im1}−Fe−N^{im2}	179.8(4)	172.9(3)	175.7(1)	178.3(2)
S(1)−Fe−S(2)	100.1(1)	94.17(9)	97.3(1)	95.30(8)
S(1)−Fe−N^{t1}	164.1(2)	175.0(2)	167.9(1)	169.2(2)
S(2)−Fe−N^{t2}	165.9(2)	179.3(2)	168.9(1)	168.9(1)
N^{im1}−Fe−S(1)	85.2(2)	86.5(2)	84.9(1)	85.9(2)
N^{im1}−Fe−N^{t1}	82.2(3)	93.6(3)	84.2(1)	84.2(2)
N^{im2}−Fe−S(1)	94.8(3)	91.1(2)	97.9(1)	95.8(2)
N^{im2}−Fe−S(2)	86.7(2)	85.5(2)	85.7(1)	87.2(2)
N^{im2}−Fe−N^{t1}	98.1(3)	89.4(3)	92.7(1)	94.2(2)
N^{im2}−Fe−N^{t2}	82.1(3)	93.8(3)	84.0(1)	83.4(2)
S(1)−Fe−N^{t2}	89.4(2)	85.8(2)	88.3(1)	90.0(2)
S(2)−Fe−N^{t1}	90.4(2)	90.8(2)	89.4(1)	89.4(2)
N^{t1}−Fe−N^{t2}	82.8(3)	89.2(3)	87.0(1)	86.9(2)

[a] Standard deviations in parentheses. [b] t1 = terminal nitrogen number 1, t2 = terminal nitrogen number 2. [c] im1 = imine nitrogen number 1, im2 = imine nitrogen number 2.

Table 3. Comparison of Electronic Spectral Data for Nitrile Hydratase Enzyme vs Model Compounds

	λ_{max} (ϵ)	
	MeCN	H_2O
$[Fe^{III}(DITpy)_2]^+$ (**1**)[a]	784 (1300)	732 (1400)
$[Fe^{III}(DITIm)_2]^+$ (**2**)[a]	802 (1300)	740 (1200)
$[Fe^{III}(ADIT)_2]^+$ (**3**)[b]	718 (1400)	693 (1400)
$[Fe^{III}(AMIT)_2]^+$ (**4**)[b,g]	696 (1100)	
inactive enzyme (pH = 9)[c,d]		690 (∼1200)
active enzyme (pH = 7.3)[c,d]		710 (∼1200)
active enzyme (butyrate-free)[e]		676 (NR)[h]
enzyme + CH_3CH_2CN[f]		690 (∼4200)

[a] This work. [b] Shoner, S. C.; Barnhart, D.; Kovacs, J. A. *Inorg. Chem.* **1995**, *34*, 4517−4518. [c] These spectra were recorded in the presence of a butyrate buffer. [d] Brennan, B. A.; Cummings, J. G.; Chase, D. B.; Turner, I. M., Jr.; Nelson, M. J. *Biochemistry* **1996**, *35*, 10068−10077. [e] Honda, J.; Kandori, H.; Okada, T.; Nagamune, T.; Shichida, Y.; Sasabe, H.; Endo, I. *Biochemistry*, **1994**, *33*, 3577−3583. [f] Sugiura, Y.; Kuwahara, J.; Nagasawa, T.; Yamada, H. *J. Am. Chem. Soc.* **1987**, *109*, 5848−5850. [g] Aqueous solution values not reported for complex **4** due to rapid decomposition in water. [h] NR = not reported.

consistent with charge-transfer bands (Table 3; Figure 5). These bands appear to be a diagnostic feature of the pseudo-octahedral *cis*-dithiolate arrangement about Fe(III) and have been tentatively assigned as Sπ → Fe(III) charge-transfer (LMCT) transitions.[30] They are particularly sensitive to the H-bonding ability of the solvent. In going from aprotic MeCN to H_2O the LMCT bands are blue-shifted to shorter wavelengths (Figure 5). In addition to solvent effects, the identity of N_{term} (py vs Im vs NH_2) also causes pronounced shifts in the position of the ∼700 nm CT band. For example, when the terminal amines of **3** and **4** are replaced with pyridine **1** or imidazole **2**, the band red-shifts to longer wavelengths (Table 3). Replacement of *gem*-dimethyl substituents on the carbon α to the thiolate carbon with hydrogens causes these bands to blue-shift (**3** vs **4** in Table 3).

(30) Kennepohl, P.; Jackson, H. L.; Schweitzer, D.; Ellison, J. J.; Shoner, S. C.; Kovacs, J. A.; Solomon, E. I. Unpublished results.

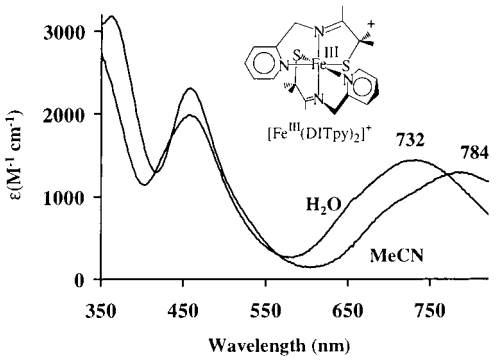

Figure 5. Electronic spectrum of $[Fe^{III}(DITpy)_2]Cl$ (**1**) in aprotic (MeCN, 298 K) vs protic (H_2O, 298 K) solvents.

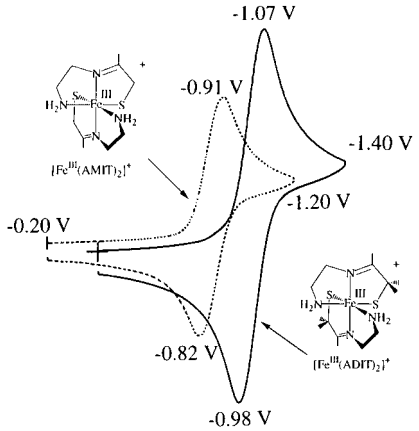

Figure 6. Cyclic voltammograms of $[Fe^{III}(AMIT)_2]^+$ (**3**) and $[Fe^{III}(AMIT)_2]Cl$ (**4**) in MeCN solution at 298 K (0.1 M $(Bu_4N)PF_6$, glassy carbon electrode, 100 mV/s scan rate). Peak potentials vs SCE are indicated.

Table 4. Redox Potentials ($E_{1/2}$ vs SCE) of Model Compounds vs Nitrile Hydratase

	DMF		CH_3CN		H_2O	
	$E_{1/2}$ (V)	ΔE (mV)	$E_{1/2}$ (V)	ΔE (mV)	$E_{1/2}$ (V)	ΔE (mV)
$[Fe^{III}(DITpy)_2]^+$ (**1**)[a]			−0.93	90	−0.74	60
$[Fe^{III}(DITIm)_2]^+$ (**2**)[a]			−0.68	350		
$[Fe^{III}(ADIT)_2]^+$ (**3**)[a]			−1.02	90	−0.77	60
$[Fe^{III}(AMIT)_2]^+$ (**4**)[a]			−0.86	90		
$[Fe^{III}(PyAS)_2]^+$ [b]	−0.13	60				
$[Fe^{III}(PyMS)_2]^+$ [b]	−0.51	NR[f]				
$[Fe^{III}(PyPepS)_2]^+$ [c]	−1.12	120				
NHase enzyme[d,e]					−0.48	NR[f]

[a] This work. [b] Noveron, J. C.; Herradora, R.; Olmstead, M. M.; Mascharak, P., K. *Inorg. Chim. Acta.* **1999**, *285*, 269−276. [c] Noveron, J. C.; Olmstead, M. M.; Mascharak, P. K. *Inorg. Chem.* **1998**, *37*, 1138−1139. [d] NHase enzyme from *Rhodococcus* sp. R312 in the presence of butyric acid. [e] Artaud, I.; Chatel, S.; Chauvin, A. S.; Bonnet, D.; Kopf, M. A.; Leduc, P. *Coord. Chem. Rev.* **1999**, *192*, 577−586. [f] NR = not reported.

Electrochemistry. Redox potentials for the Fe(III)/Fe(II) redox couple for complexes **1**−**4** are summarized in Table 4. As illustrated in the cyclic voltammograms of **3** and **4** (Figure 6), complexes **1**, **3**, and **4** are reversibly reduced in acetonitrile. Half-wave potentials ($E_{1/2}$) vary from −0.86 V (for **4**) to −1.02 V (for **1**) vs SCE. Complex **2** exhibits an irreversible reduction wave with an $E_{1/2}$ of −0.68 V (ΔE = 350 mV) vs SCE. This is likely a consequence of the more flexible propylene linker, which may facilitate the dissociation of one or both terminal imidazole groups in the reduced species. Complexes **1** and **3** are also reversibly reduced in aqueous solution (complexes **2**

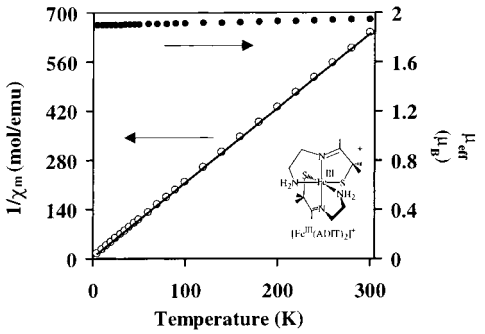

Figure 7. Temperature dependence of the reciprocal molar susceptibility ($1/\chi_m$) (○) and effective magnetic moment (μ_{eff}) (●) of polycrystalline $[Fe^{III}(AMIT)_2]Cl$ (**3**). Solid line represents fit of the susceptibility data to the Curie−Weiss law ($C = 0.471$, $\theta = -2.08$).

Table 5. EPR Parameters for Model Compounds vs Nitrile Hydratase

	g values		
$[Fe^{III}(DITpy)_2]^+$ (**1**)[a]	2.16	2.10	2.02
$[Fe^{III}(DITIm)_2]^+$ (**2**)[a]	2.19	2.15	2.01
$[Fe^{III}(ADIT)_2]^+$ (**3**)[b]	2.19	2.13	2.01
$[Fe^{III}(AMIT)_2]^+$ (**4**)[b]	2.20	2.16	2.00
$[Fe^{III}(PyAS)_2]^+$ [c]	2.17	2.11	2.01
$[Fe^{III}(PyMS)_2]^+$ [c]	2.13	2.09	2.03
$[Fe^{III}(PyPepS)_2]^+$ [d]	2.22	2.14	1.98
NHase enzyme + N_3^- [e,g]	2.23	2.14	1.99
NHase enzyme (pH = 9)[e,f,h]	2.20	2.12	1.99
NHase enzyme (pH = 7.3)[e,f,h]	2.27	2.14	1.97
NHase enzyme + $(CH_3)_2CHCN$ (pH = 7.2)[e,g]	2.21	2.12	1.98

[a] This work. [b] Shoner, S. C.; Barnhart, D.; Kovacs, J. A. *Inorg. Chem.* **1995**, *34*, 4517−4518. [c] Noveron, J. C.; Herradora, R.; Olmstead, M. M.; Mascharak, P., K. *Inorg. Chim. Acta.* **1999**, *285*, 269−276. [d] Noveron, J. C.; Olmstead, M. M.; Mascharak, P. K. *Inorg. Chem.* **1998**, *37*, 1138−1139. [e] These spectra were recorded in the presence of a butyrate buffer, which was added in order to stabilize the samples. Butyrate appears to act as an inhibitor. [f] The reported *g*-values are those of a "butyrate-inhibited" form of the enzyme. [g] Sugiura, Y.; Kuwahara, J.; Nagasawa, T.; Yamada, H. *J. Am. Chem. Soc.* **1987**, *109*, 5848−5850. [h] Brennan, B. A.; Cummings, J. G.; Chase, D. B.; Turner, I. M., Jr.; Nelson, M. J. *Biochemistry* **1996**, *35*, 10068−10077.

and **4** were too unstable in water to obtain reproducible potentials). As shown in Table 4, potentials shift, by as much as 250 mV, to more positive potentials in water.

Magnetic Properties. The magnetic susceptibility for complexes **1**−**4** follow the Curie−Weiss law over a wide temperature range. This is illustrated in the $1/\chi_m$ (χ_m = molar magnetic susceptibility) vs temperature (T) plot for complex **3** in Figure 7, which can be fit to an $S = {}^1/_2$ spin state over the temperature range 5−300 K. Effective moments obtained from fits of $1/\chi_m$ vs T plots for compounds **1**−**4** (range: $\mu_{eff} = 1.72$ (**4**) to 1.91 (**3**) μ_B) are close to the spin-only value ($\mu_{eff} = 1.73\,\mu_B$) for one unpaired electron. There are no thermally accessible, higher spin states within the temperature range studied. The room temperature magnetic moments obtained by Evan's method[21,22] are also consistent with a low-spin ($S = {}^1/_2$) ground state for complexes **1**−**4**. This is further supported by the EPR spectra of complexes **1**−**4** (Table 5 and Figure 8), which are typical of a low-spin ($S = {}^1/_2$) Fe(III) center in a distorted octahedral ligand field. The rhombic EPR spectrum of **1**, shown in Figure 8, closely resembles those of complexes **2**−**4** and displays a fairly narrow *g*-spread ($\Delta g = g_{max} - g_{min} = 0.14$).

Structural Effects on Redox and Electronic Spectral Properties. Changes in the local environment near the metal center, including perturbations at the periphery of the ligand,

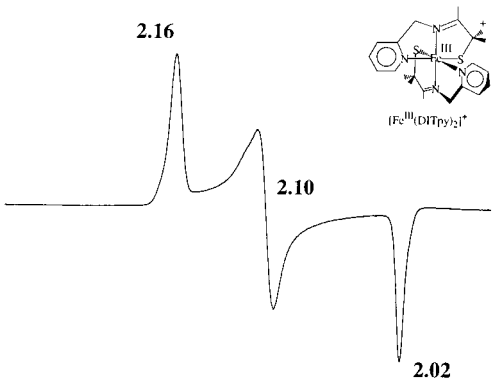

Figure 8. X-band EPR spectrum of $[Fe^{III}(DITpy)_2]Cl$ (**1**) in MeOH/EtOH (9:1) glass at 135 K. Microwave frequency: 9.419 GHz. Microwave power: 2 mW. Modulation frequency: 100 kHz. Modulation amplitude: 2 G.

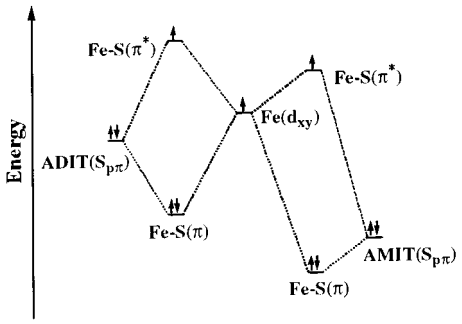

Figure 9. Simplified partial MO diagram for *gem*-dimethyl-substituted ADIT (**3**) and AMIT (**4**) illustrating the differential $S\pi$-Fe(d_{xy}) bonding and antibonding interactions.

changes in the primary ligating atoms, and changes in solvent all have pronounced effects on both the redox and electronic spectral properties of complexes **1**−**4**. In going from *gem*-dimethyls in **3** to *gem*-dihydrogens in **4** both the $E_{1/2}$ and the λ_{max} show pronounced shifts in energy. In MeCN solution, the $E_{1/2}$ shifts cathodically by 160 mV (Figure 6), while the λ_{max} of the low-energy CT band blue-shifts by 22 nm, from 718 to 696 nm (Table 3). These results can be rationalized with a simple MO diagram (Figure 9). Placement of electron-releasing *gem*-dimethyl groups (in **3**) on the carbon α to the thiolate raises the energy of the sulfur π-symmetry p-orbitals so that they lie energetically closer to the metal's π-symmetry orbital (d_{xy}). This enables a better energy match between the sulfur orbitals on **3** vs **4** and the d_{xy} orbital on iron. This results in a greater destabilization of the d_{xy}(Fe−S(π*)) orbital and greater stabilization of the Sπ(Fe−S(π)) orbital, which is mainly sulfur in character, for $[Fe^{III}(ADIT)_2]^+$ (**3**) relative to $[Fe^{III}(AMIT)_2]^+$ (**4**). As a result, the mean Fe−S distance is longer in $[Fe^{III}(AMIT)_2]^+$ (2.232(2) Å) vs $[Fe^{III}(ADIT)_2]^+$ (2.20(1) Å). It is also more difficult to reduce the compound containing the more electron-rich ADIT ligand as a consequence of its more destabilized HOMO d_{xy}. The *gem*-dimethyl substituents increase the electron-donating ability of the adjacent thiolate sulfurs, which provides for a thermodynamically more stable complex. The charge-transfer band near 700 nm for all four complexes examined in this study (Table 3), and NHase,[11,12] probably involves a transition between the Sπ(Fe−S(π)) and the d_{xy}(Fe−S(π^*)) orbitals. This transition is 22 nm (1.3 kcal/mol) lower in energy for $[Fe^{III}(ADIT)_2]^+$ vs $[Fe^{III}(AMIT)_2]^+$ since the ligand sulfur orbitals ($S_{p\pi}$) from which the Sπ(Fe−S(π)) originates start out higher in energy. In other words, ligand-to-metal charge transfer from the more electron rich sulfurs ($(Me_2)C-S^-$) in

$[Fe^{III}(ADIT)_2]^+$ occurs at lower energies than from the less electron rich sulfurs (H_2C-S-) in $[Fe^{III}(AMIT)_2]^+$.

The orthogonal orientation of both the pyridine and imidazole rings of structures **1** and **2** are of the proper symmetry to allow the imidazole-π^* and pyridine-π^* orbitals to π-overlap with the metal's d_{xy} orbital. This π-back-bonding interaction would result in a net stabilization of the HOMO d_{xy} orbital for both complexes. Shifts in the redox potential (in MeCN solution) (Table 4) for complexes **1** ($\Delta E_{1/2}$= 90 mV) and **2** (($E_{1/2} - E_{pc}$) = 170 mV) relative to **3** are consistent with pyridine and imidazole behaving as π-acceptors. However, this π-overlap must be moderate, since it is not significant enough to be noticed in the solid-state structures. The red-shifts (in MeCN solution) of the low-energy charge-transfer band of **1** ($\Delta\lambda_{max}$ = 66 nm) and **2** ($\Delta\lambda_{max}$ = 84 nm) relative to **3** is also consistent with pyridine and imidazole behaving as π-acceptors and stabilizing the d_{xy} orbital.

Solvent Effects on Redox and Electronic Spectral Properties. Protic solvents influence both the redox potentials and electronic spectral properties of **1**−**4**. Redox potentials display a cathodic shift (Table 4) and the low-energy charge-transfer band blue-shifts (Table 3) in protic solvents. A likely explanation for this is that the thiolate sulfurs are hydrogen bonding (H-bonding) to solvent. This would stabilize any molecular orbital possessing sulfur character, including both the HOMO d_{xy}(Fe−S(π^*)) and the Sπ(Fe−S(π)) orbitals. Since these two orbitals are involved in the charge-transfer transition observed near 700 nm, one would expect the energy of this transition to be affected, as long as the net H-bonding-induced stabilization is not identical for the two orbitals. The observed blue-shifts (Table 3) imply that the lower energy orbital, Sπ(Fe−S(π)), is stabilized more than the higher energy one, d_{xy}(Fe−S(π^*)). One would expect the orbital with greater sulfur character (i.e., Sπ(Fe−S(π)) bonding MO), to be more affected by H-bonding than the orbital with less sulfur character (i.e., the HOMO d_{xy}(Fe−S(π^*))). The cathodic shift in redox potential provides evidence for the stabilization of the HOMO d_{xy} orbital in H-bonding solvents. Or, viewed differently, because protic solvents stabilize the ligand thiolate sulfur orbitals via H-bonding, a poorer overlap between the metal d_{xy} and sulfur p-orbital would result, and consequently there would be less destabilization of the anti-bonding d_{xy}(Fe−S(π^*)), resulting in a more cathodic redox potential. Recent XAS studies by Hodgson and co-workers[31] on rubredoxin proteins and a rubredoxin model complex provide support for the notion that hydrogen-bonding interactions can cause a decrease in the covalency of an Fe−thiolate bond. Pronounced cathodic shifts in redox potential are also observed with model complexes of the thiolate-ligated heme enzyme cytochrome P450 as a consequence of H-bonding interactions to the coordinated thiolate ligand.[32]

Influence of Sulfurs on the Spin State. Most Fe(III) complexes are either high-spin or in spin-equilibrium.[33] There is, however, a slowly growing body of low-spin Fe(III) thiolate complexes (Table 5).[6a,b,f,h,l] A possible explanation for the low-spin ground state in these complexes is that the Fe(III) thiolate bonds are highly covalent. If enough electron density is transferred from the sulfurs to the Fe(III) center, the effective positive charge on the metal would be reduced, allowing for an expansion of the d orbitals. This expansion would result in a decrease in the interelectronic repulsions within the d-orbital manifold that could be reduced to a point in which the low-spin state is favored over higher spin states. This effect is commonly known as central field covalency,[34] and is one of the mechanisms that cause the nephelauxetic effect.[35] Thiolates are known to be effective electron donors.[34] The low-energy charge-transfer bands are a reflection of the covalency of the Fe(III)−thiolate bonds in both the complexes described herein and in NHase.[36] Electron delocalization onto the ligands, along with an asymmetric ligand field, serves to partially quench the orbital angular momentum contribution to the magnetic moment.[37] This results in a smaller *g*-spread than is typically seen in $S = {}^1/_2$ Fe(III) complexes such as ferriheme centers[38] which typically display *g*-spreads of ≥ 0.5.

Relation to NHase Active Site. The S$\pi \rightarrow$ Fe(III) CT absorption in complexes **1**−**4** appears to be a sensitive reporter of perturbations to not only the primary coordination sphere but also the secondary coordination sphere, (i.e., the ligand's periphery as well as solvent). The electronic spectrum of nitrile hydratase is also sensitive to changes to its secondary coordination sphere (e.g., the pH, Table 3).[12] In going from pH = 7.3 to pH = 9 the low-energy CT absorption present in the enzyme is blue-shifted from 710 to 690 nm. This blue shift was attributed to a loss of H-bonding interactions to the coordinated cysteinate residues.[12] Results described herein suggest, however, that if this were the case, then the CT band should red-shift, as opposed to blue-shift.

The electrochemical results described herein show that the combination of imine nitrogens and alkyl thiolate donors are capable of stabilizing the Fe(III) oxidation state and are within the range reported for similar complexes (Table 4).[6a,h] Artaud and co-workers reported an $E_{1/2}$ of −480 mV vs SCE for Fe-NHase (Table 4).[6g] It is not surprising that the reduction potentials (in MeCN) of our models **1**−**4** are more negative than the reduction potential reported for the enzyme, since our models lack the secondary interactions present in metalloenzymes, such as H-bonding interactions. This has been observed with iron−sulfur cluster models as well.[36,39] The observed cathodic shift in $E_{1/2}$ values for **1** and **3** in aprotic MeCN vs aqueous solution support this conclusion. The results obtained from the present study therefore support previous studies[40] that have shown that H-bonding interactions between a protein and a metal-containing active site may significantly affect the redox potentials and electronic spectral properties. It should also be pointed out that the lower reduction potential of Fe-NHase could also be a result of the ligated Cys-SO_n (n = 1, 2) units. Darensbourg and co-workers have shown that S-oxygenation of metal-bound thiolates results in less negative reduction potentials.[41]

(31) Rose, K.; Shadle, S. E.; Eidsness, M. K.; Kurtz, D. M., Jr.; Scott, R. A.; Hedman, B.; Hodgson, K. O.; Solomon, E. I. *J. Am. Chem. Soc.* **1998**, *120*, 10743−10747.

(32) Suzuki, N.; Higuchi, T.; Urano, Y.; Kikuchi, K.; Uekusa, H.; Ohashi, Y.; Uchida, T.; Kitagawa, T.; Nagano, T. *J. Am. Chem. Soc.* **1999**, *121*, 11571−11572.

(33) (a) Greenwood, N. N.; Earnshaw, A. In *Chemistry of the Elements*; Pergamon Press: New York, 1984; p 1266. (b) Cotton, F. A.; Wilkinson, G. In *Advanced Inorganic Chemistry*; 4th ed.; Wiley: New York, 1980; pp 648−649 and 761−762. (c) Leipoldt, J. G.; Coppens, P. *Inorg. Chem.* **1973**, *12*, 2269−2274.

(34) Lever, A. B. P. In *Inorganic Electronic Spectroscopy*, 2nd ed.; Elsevier Science: New York, 1984; pp 736−786.

(35) Schaffer, C. E.; Jorgensen, C. K. *J. Inorg. Nucl. Chem.* **1958**, *8*, 143.

(36) Holm, R. H.; Kennepohl, P.; Solomon, E. I. *Chem. Rev.* **1996**, *96*, 2239−2314.

(37) Figgis, B. N. In *Introduction to Ligand Fields*; John Wiley & Sons: New York, 1966; p 276.

(38) Walker, F. A. *Coord. Chem. Rev.* **1999**, *185*−*186*, 471−534.

(39) Stephens, P. J.; Jollie, D. R.; Warshel, A. *Chem. Rev.* **1996**, *96*, 2491−2513.

(40) Backes, G.; Mino, Y.; Loehr, T. M.; Meyer, T. E.; Cusanovich, M. A.; Sweeney, W. V.; Adman, E. T.; Sanders-Loehr, J. *J. Am. Chem. Soc.* **1991**, *113*, 2055−2064.

The HOMO for **1**−**4** is likely the d_{xy} orbital (where the *z*-axis is defined as the $N_{im}-Fe-N_{im}$ bond axis). This matches the HOMO that has been reported for the NHase enzyme.[12] The EPR spectra of **1**−**4** most closely resemble the high-pH (pH = 9.0) form of NHase. In going from pH = 7.3 to pH = 9.0, the *g*-spread of NHase decreases from 0.30 to 0.21. This change, along with the blue-shifting of the low-energy CT band, has been attributed to a loss of H-bonding interactions, which results in an increase in the energy of the HOMO d_{xy} relative to the nonbonding d_{xz} and d_{yz} orbitals, thereby further quenching the orbital contribution, which subsequently leads to a smaller *g*-spread. While the results obtained from the present study provide support for the notion that a loss of H-bonding interactions to an Fe(III)-bound thiolate can increase the covalency of the bond, these data suggest that the changes observed with the enzyme in going from pH = 7.3 to pH = 9.0[12,13] are more complex than simply the loss of H-bonding interactions.

Summary and Conclusions

As shown by the redox potentials of **1**−**4**, alkyl thiolates, in combination with imine nitrogens, stabilize the +3 oxidation state of iron. *gem*-Dimethyl substituents on the carbons adjacent to the sulfurs provide added thermodynamic stability, as well as steric protection that prevents oligomer formation. Minor changes to either the primary or secondary coordination sphere have a dramatic influence on the electronic and redox properties of Fe(III)−thiolate complexes. The results obtained from this work show that Fe(III) in a pseudo-octahedral environment consisting of two *cis*-thiolate donors and four nitrogen donors reproduces the spectroscopic and spin-state properties of the Fe(III) center of nitrile hydratase.

Acknowledgment. We thank Dirk Schweitzer, Wendy Taylor, and Jason Shearer for helpful discussion, Tamara Okonogi for assistance with the EPR work, and Reeza Loloee for collection of SQUID magnetic susceptibility data for **4**. Financial support from the National Institutes of Health (Grant GM 45881) and the National Institute of Environmental Health Sciences (P30 ES07033; EPR spectrometer) is also gratefully acknowledged.

Supporting Information Available: Additional tables: crystallographic data, atomic positional and thermal parameters, bond distances and angles, and calculated hydrogen atom positional parameters, for **1**, **2**, and **4**. Supplemental figures include electronic spectra of **2** (Figure S1), cyclic voltammograms of **1** and **2** in MeCN and **1** and **3** in H_2O (Figures S2−S5), EPR spectrum of **2** (Figure S6), and $1/\chi_m$ vs temperature plots for **1**, **2**, and **4** (Figures S7−S9). This material is available free of charge via the Internet at http://pubs.acs.org.

IC001271D

(41) Grapperhaus, C. A.; Darensbourg, M. A. *Acc. Chem. Res.* **1998**, *31*, 451−459.